

Determining the Astrometric Error in CSC Source Positions

Arnold Rots, SAO

Introduction

The source positions in the Chandra Source Catalog (CSC) are characterized by error ellipses (circles for Version 1 of the CSC) which are based on the spatial distribution of the photons for an individual source detection. In the case of multiple detections of the same source the error ellipse is derived from the error ellipses associated with the individual detections. These error ellipses provide a good measure of the statistical uncertainty of the location of the source in the frame of the observation, but leave out a series of potential sources of error that are external to the observation:

- The error in the mean aspect solution for the observation; clearly, the effect of this error will be diminished when multiple detections of the same source are combined.
- The calibration of the geometry of the spacecraft, in particular the optical axes of the aspect camera and the HRMA.
- The astrometric errors in the Guide Star Catalog; this should be very small.
- The calibration of the geometry of the focal plane, its projection on the detectors, and the distortions therein.

For all practical purposes, we shall combine these errors and call it an astrometric systematic error, even though not all of its components are truly systematic. The intent of this study is to derive the value of this compound quantity in order to add it to the CSC statistical position error to obtain a reliable absolute error for each of the CSC sources.

Procedure

The CSC-SDSS cross-match catalog contains 7989 objects that are classified as stars in the SDSS catalog. Since these sources are, by their nature, point-like we assume their optical and X-ray positions to be well-determined and coincident. We have further narrowed the sample down by requiring the match probability to be greater than 90%. The resultant sample contains 6310 CSC-SDSS object pairs which are uniquely associated with 9476 sources detected in individual observations; these 9476 objects were used for this analysis. By using the combined spatial error estimate of each object pair as independent variable and analyzing the statistical distribution of the measured separations, it is possible to derive the value of the missing astrometric error in the CSC. The assumption here is that the astrometric error is relatively small compared to the CSC uncertainties, especially off-axis, and will therefore mainly affect the pairs with small combined errors.

The separation is a single-axis radial measure and, in order to perform the analysis correctly, the positional uncertainties also need to be converted to a single-axis radial quantity. CSC provides the major and minor axes of an error ellipse, while the SDSS gives independent errors in RA and Dec, which are also assumed to represent an error ellipse. The combined error is then derived by adding the geometric means of the major and minor axes for CSC and SDSS in quadrature; in other words: the square root of the sum (CSC plus SDSS) of the products of major and minor axis. We want to be dealing with 1- σ values and since the CSC error ellipses refer to a 95% confidence level, the CSC values are to be multiplied by 0.408539.

To put all this in mathematical expressions:

- ϵ_0 : semi-major axis of CSC 95% confidence ellipse
- ϵ_1 : semi-minor axis of CSC 95% confidence ellipse
- σ_{RA} : 1- σ error in RA for SDSS positions
- σ_{Dec} : 1- σ error in Dec for SDSS positions
- σ_c : 1- σ combined statistical radial position error for CSC-SDSS cross-matches
- σ_a : 1- σ astrometric error
- σ'_c : 1- σ combined corrected statistical radial position, including astrometric error
- ρ : (radial) separation of CSC and SDSS positions for a cross-match pair: measured error
- $\rho_N(\sigma)$: normalized sample error
- $\tilde{\chi}^2$: reduced χ^2

$$\sigma_c = \sqrt{0.1669041 \cdot \epsilon_0 \cdot \epsilon_1 + \sigma_{RA} \cdot \sigma_{Dec}}$$

$$\sigma'_c = \sqrt{0.1669041 \cdot \epsilon_0 \cdot \epsilon_1 + \sigma_{RA} \cdot \sigma_{Dec} + \sigma_a^2}$$

$$\rho_N(\sigma) = \frac{\rho}{\sigma}$$

$$\tilde{\chi}^2 = \frac{\sum_1^n \rho_N^2}{n - 1}$$

In the following, σ_c (or σ'_c) is the independent variable, ρ or ρ_N the dependent variable. All values are in units of arcsecond.

Analysis

After sorting the data in increasing order of σ_N we calculated $\tilde{\chi}^2(\rho_N(\sigma_c))$ for bins of, successively, 100, 200, 300, 400, 500, 500, ..., 500, and 476 sources, and plotted it against the mean value of σ_c for the bin. The result is shown in Fig. 1a. The values at $\sigma_c > 0.25$ are quite reasonable, but the steep rise below this value is indicative of an error component that is of that order. We interpret this as caused by the missing astrometric error discussed in the Introduction. Our assertion is that, if the left hand part of the curve can be flattened out by adding a suitable value for σ_a in σ'_c and using that value in the calculation of $\rho_N(\sigma'_c)$ and $\tilde{\chi}^2(\rho_N(\sigma'_c))$, one has determined the astrometric error. A value of $\sigma_a = 0.16''$ (± 0.01) provides

a good result as shown in Fig. 1b. For comparison, the same plot for values of $\sigma_a = 0.15''$ and $\sigma_a = 0.17''$ is presented in Figs. 1c and 1d, respectively.

To verify the reliability of the result, we plotted the distribution of ρ_N in three ranges of the independent variable: $\sigma_c < 0.15$, $0.25 < \sigma_c < 1.0$, and $1.0 < \sigma_c$ (Figs. 2a, 3a, 4a). We expect these to show Rayleigh distributions; they do, but the one in Fig. 2a is significantly shifted toward higher values, as is to be expected. When we make the same plots again, using σ'_c and $\rho_N(\sigma'_c)$ instead (see Figs. 2b, 3b, 4b), the distributions all match. The distribution of $\rho_N(\sigma'_c)$ for the entire sample is shown in Fig. 5.

In Fig. 6 we plot, for the bins from Fig. 1, the average off-axis angle θ (in arcminutes) against the average estimated error, including the 0.16 arcsec systematic error. As expected, small errors are predominantly found at small off-axis angles, large ones at large angles. Fig. 9 may provide a more useful representation, using θ as the independent parameter and plotting the measured error ρ as the dependent parameter.

Finally, in Fig. 7 we plot, for the bins from Fig. 1, the average source separation ρ against the average estimated error σ'_c , including the 0.16 arcsec systematic error; the dashed black line represents the identity relation. The figure shows that ρ tracks σ'_c quite well. But the divergence at higher values of σ'_c indicates that the statistical errors of the CSC positions are likely to be overestimated when those errors are large; this corresponds (cf. Fig. 6) to off-axis angles greater than 7 or 8 arcmin. The same phenomenon can be observed in Fig. 1b where the plot slopes down for large values of the error.

Conclusion

Our conclusion is that the astrometric error in CSC positions, resulting from the four components listed in the Introduction, is $0.16'' \pm 0.01''$. Adding this value in quadrature to the current error will result in a reliable value for the absolute position errors in the CSC. We recommend that the determination of the statistical errors for off-axis sources be investigated further.

Acknowledgments

I thank Tamàs Budavári and Alex Szalay for providing the SDSS end of the data and the cross-match algorithm, and Frank Primini and Kenny Glotfelty for very helpful discussions.

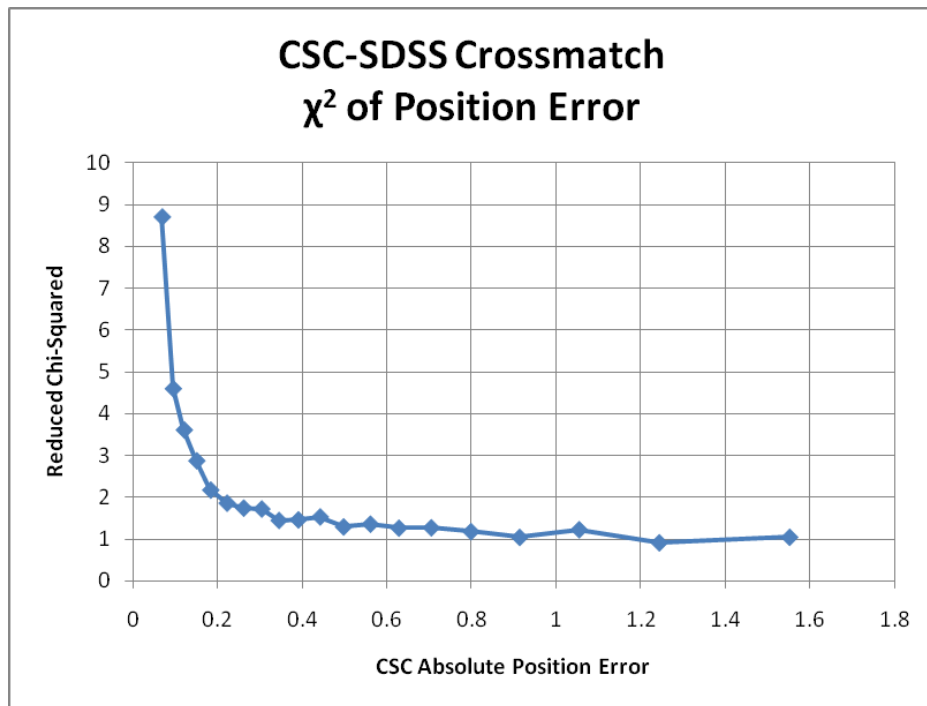


Fig. 1a $\tilde{\chi}^2 (\rho_N(\sigma_c))$ as a function of σ_c for bins of 100, 200, 300, 400, 500, ... , 500, 476 sources.

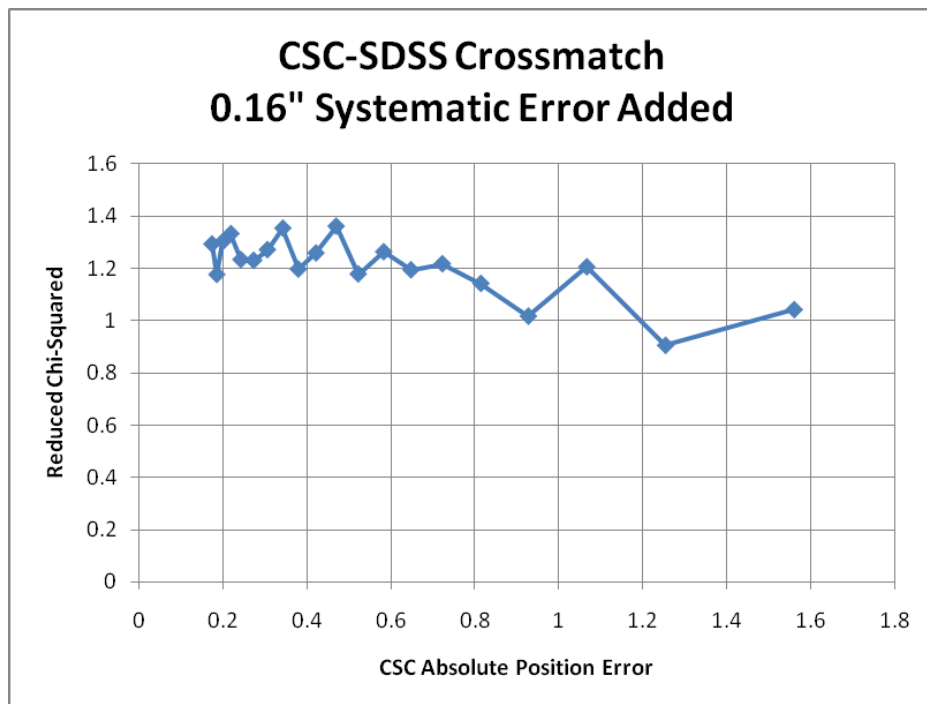


Fig. 1b $\tilde{\chi}^2 (\rho_N(\sigma'_c))$ as a function of σ'_c for bins of 100, 200, 300, 400, 500, ... , 500, 476 sources, where $\sigma_a=0.16$ arcsec.

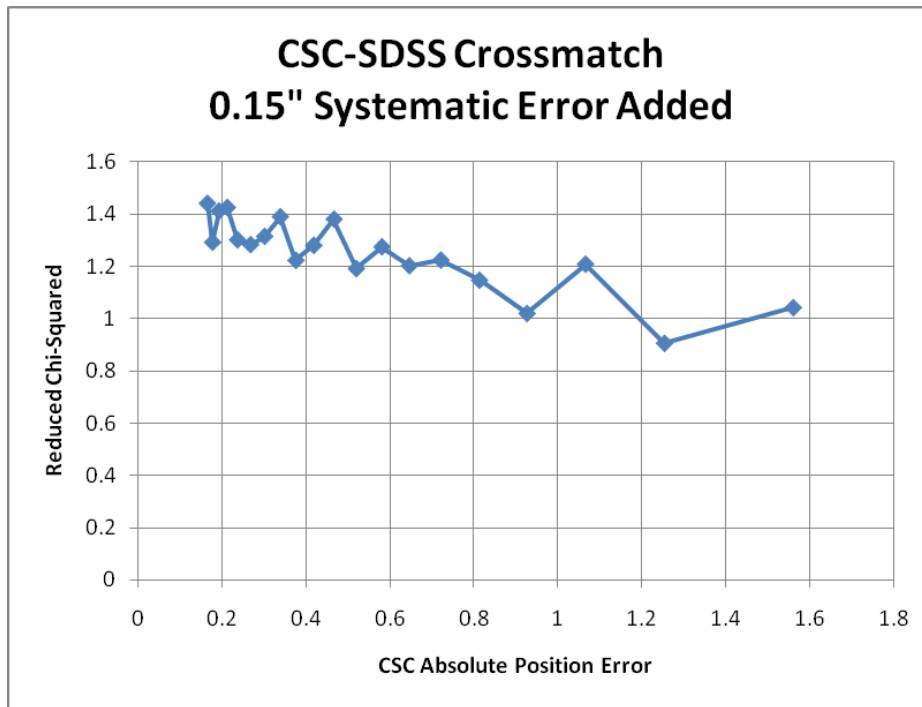


Fig. 1c $\tilde{\chi}^2 (\rho_N(\sigma'_c))$ as a function of σ'_c for bins of 100, 200, 300, 400, 500, ... , 500, 476 sources, where $\sigma_a=0.15$ arcsec.

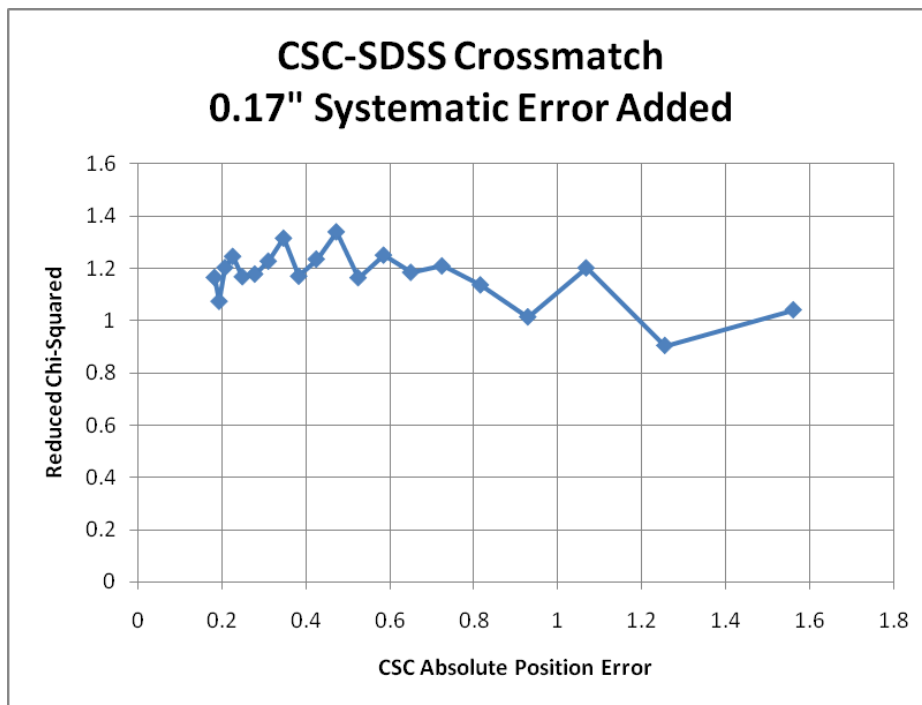


Fig. 1d $\tilde{\chi}^2 (\rho_N(\sigma'_c))$ as a function of σ'_c for bins of 100, 200, 300, 400, 500, ... , 500, 476 sources, where $\sigma_a=0.17$ arcsec.

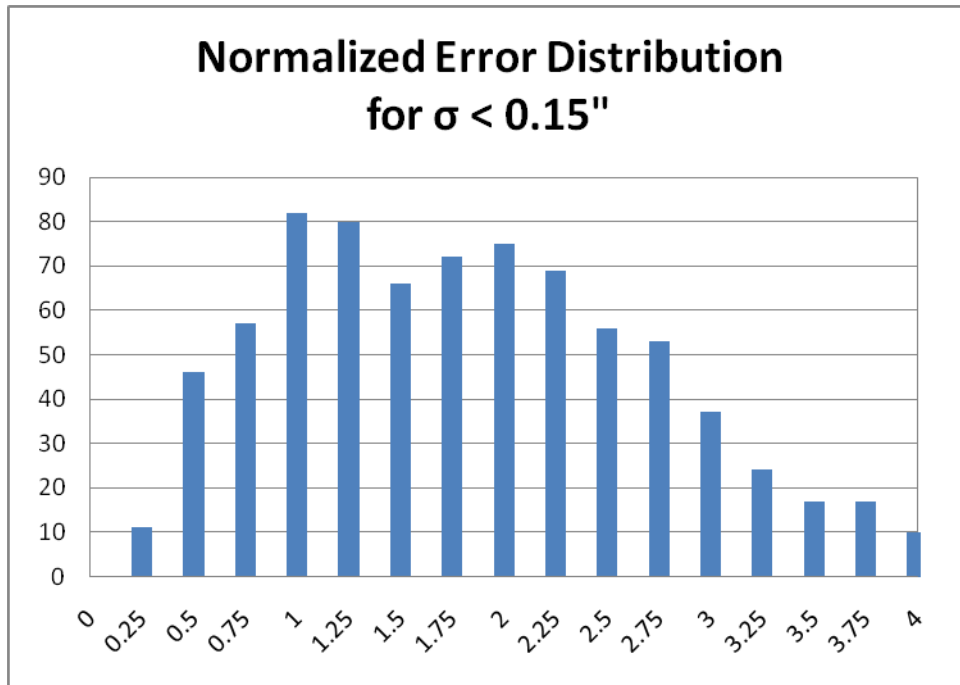


Fig. 2a The distribution of $\rho_N(\sigma_c)$ as a function of σ_c for $\sigma_c < 0.15''$. Note that the Rayleigh distribution is clearly shifted to the right.

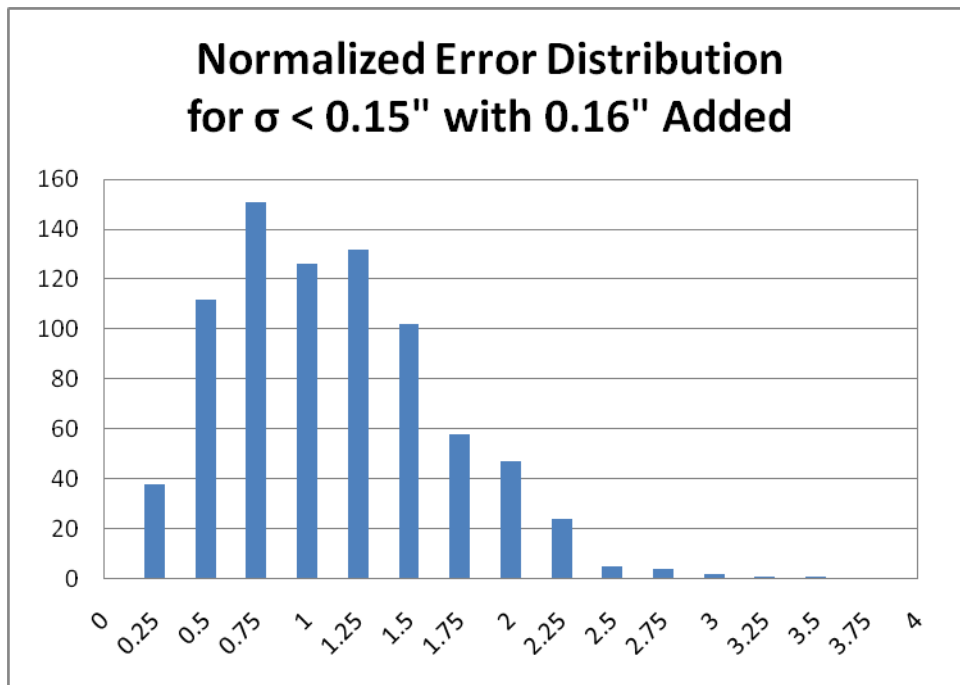


Fig. 2b The distribution of $\rho_N(\sigma'_c)$ as a function of σ'_c for $\sigma_c < 0.15''$. Note that the Rayleigh distribution agrees with those in Figs. 3 and 4.

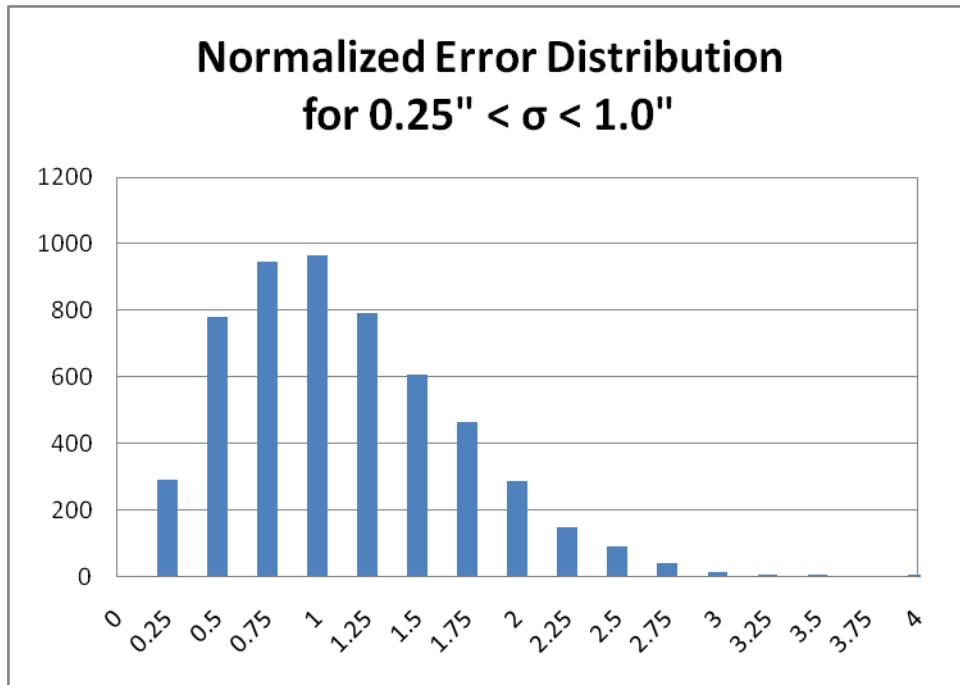


Fig. 3a The distribution of $\rho_N(\sigma_c)$ as a function of σ_c for $0.25'' < \sigma_c < 1.0''$. Note that the Rayleigh distribution is similar to that in Fig. 4a and as expected for a correct distribution.

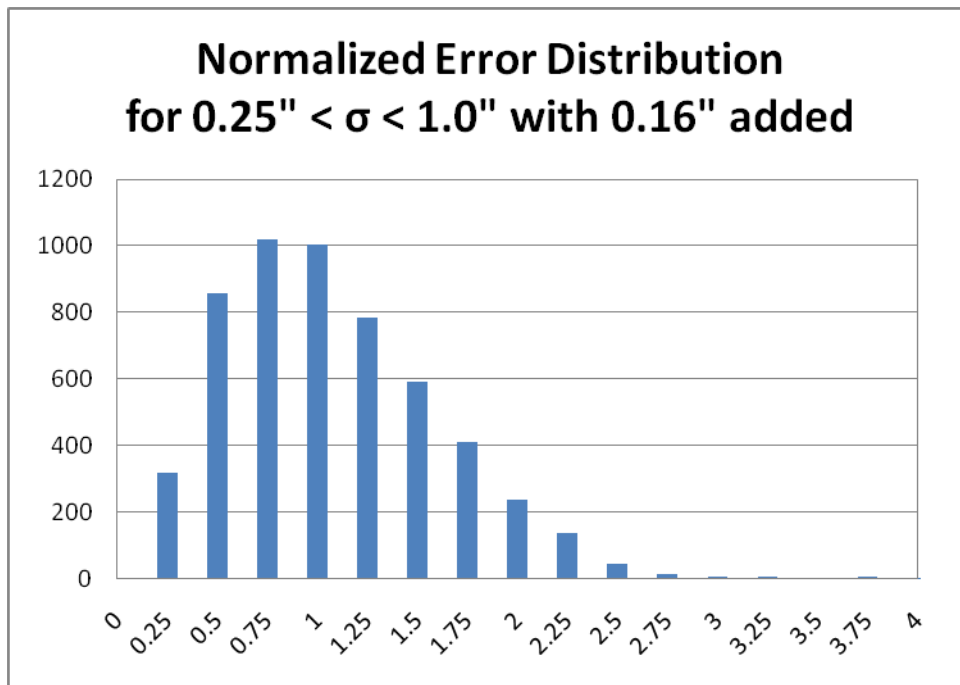


Fig. 3b The distribution of $\rho_N(\sigma'_c)$ as a function of σ'_c for $\sigma_c < 0.15''$. Note that the Rayleigh distribution is fairly similar to the one in Fig. 3a.

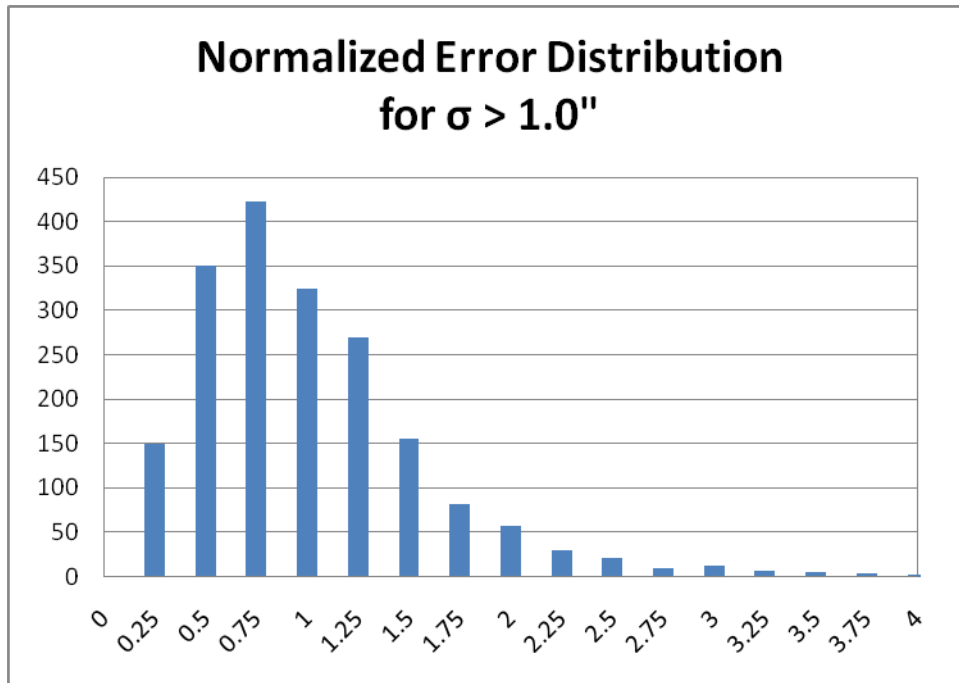


Fig. 4a The distribution of $\rho_N(\sigma_c)$ as a function of σ_c for $\sigma_c > 1.0''$. This Rayleigh distribution is as expected for correct error values.

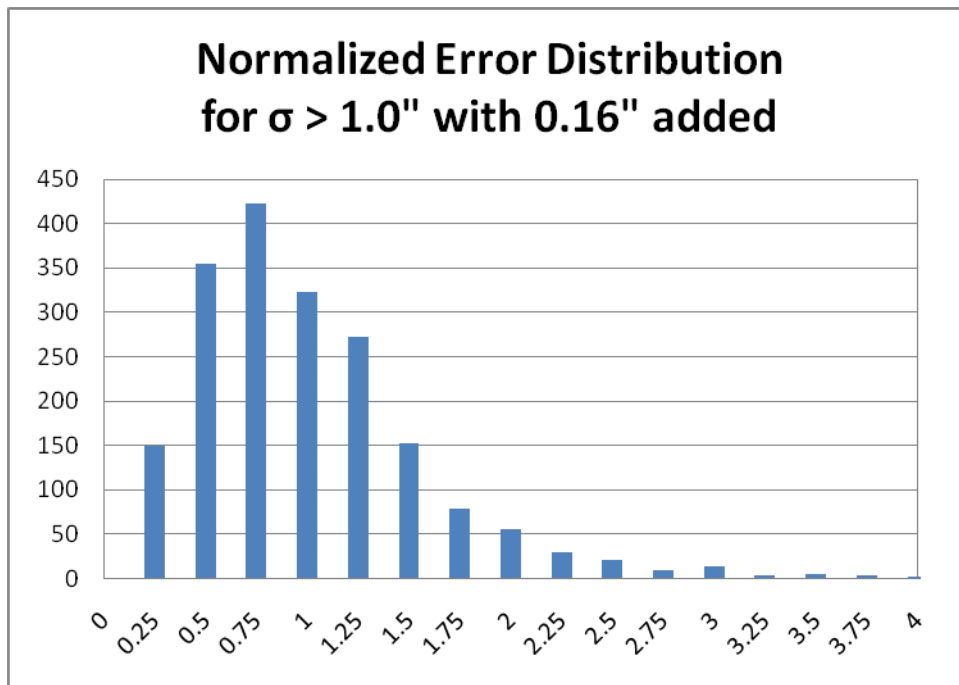


Fig. 4b The distribution of $\rho_N(\sigma'_c)$ as a function of σ'_c for $\sigma_c < 0.15''$. Note that the Rayleigh distribution is very similar to the one in Figs. 4a, 2b, and 3b.

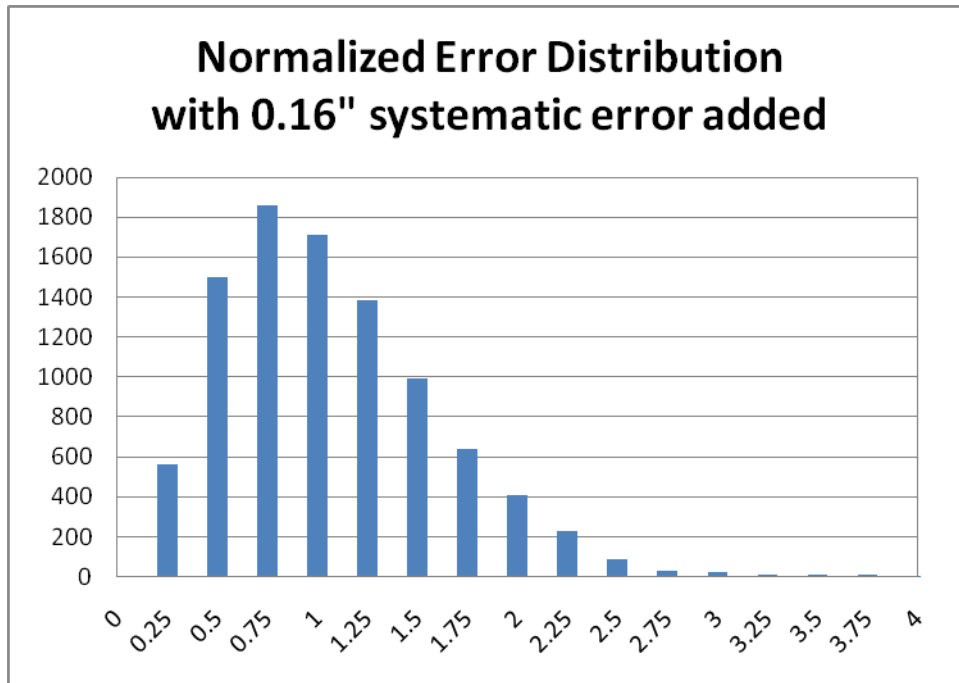


Fig. 5 The distribution of $\rho_N(\sigma'_c)$ as a function of σ'_c for all values of σ_c .

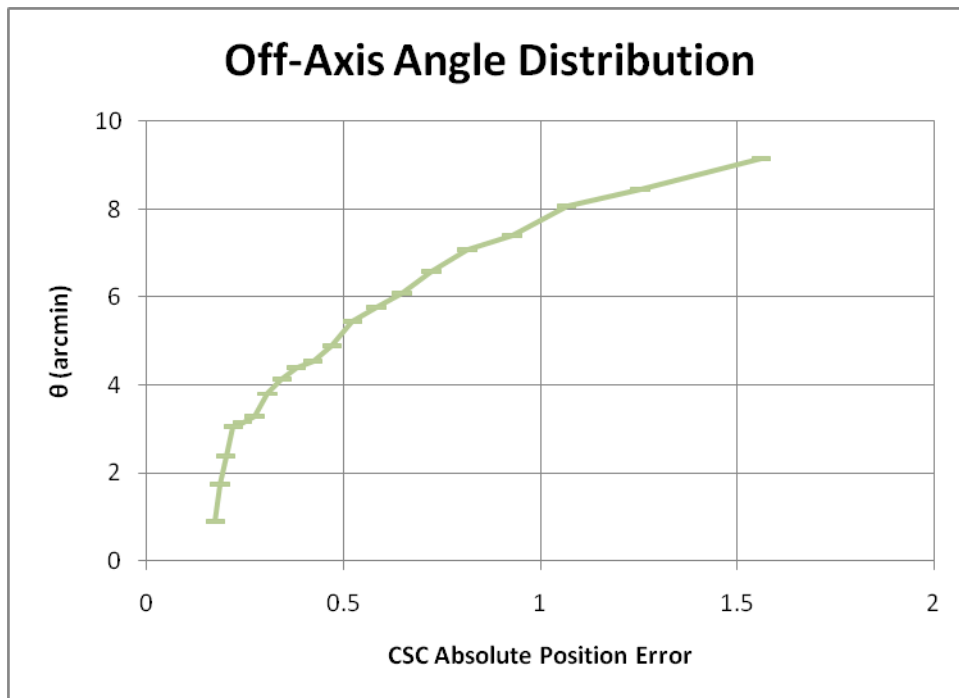


Fig. 6 The average values of off-axis angle θ for the bins from Fig. 1, with a systematic error of 0.16'' added.

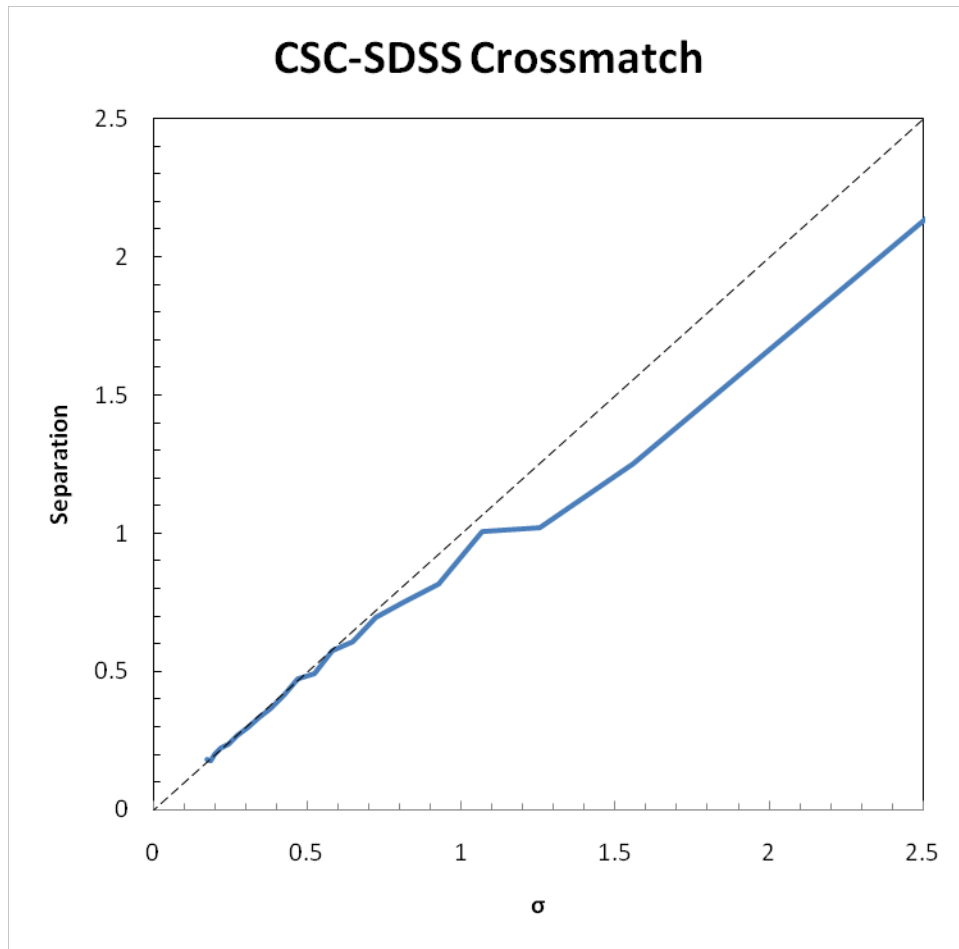


Fig. 7 The average value of the source separation, ρ , versus the average value of the estimated error (including a $0.16''$ astrometric systematic error) from the bins in Fig. 1. The dashed black line indicates the identity function. The divergence at higher values in this plot (as well as the corresponding slope in Fig. 1b) hints that the position errors at off-axis angle greater than $7-8'$ (see Fig. 6) may be overestimated.

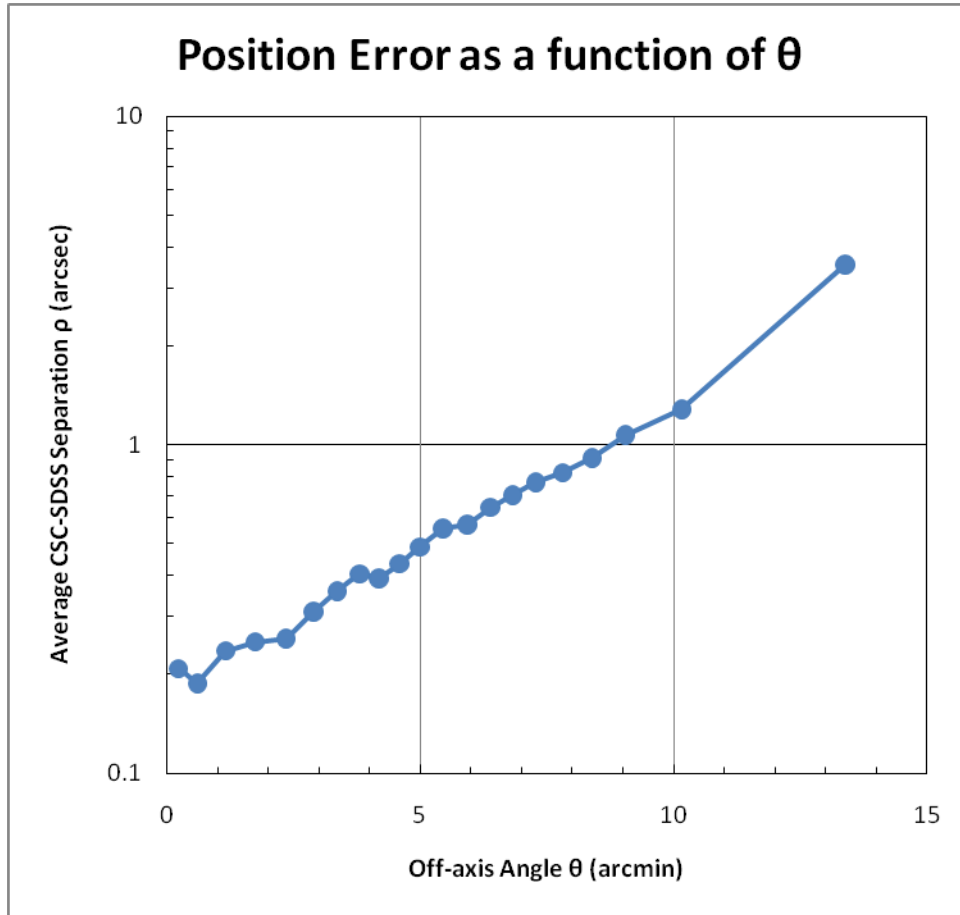


Fig. 8 The measured position error (i.e., CSC-SDSS separation ρ ; in arcsec) as a function of off-axis angle θ (in arcmin) averaged in bins of 100, 200, 300, 400, 500,..., 500, 476 source pairs, ordered by θ .